Final Draft
of the original manuscript:

Scheider, I.; Brocks, W.:
Residual strength prediction of a complex structure using crack extension analyses
In: Engineering Fracture Mechanics (2008) Elsevier

DOI: 10.1016/j.engfracmech.2008.02.009

Residual strength prediction of a complex structure using crack extension analyses

Ingo Scheider, Wolfgang Brocks

GKSS Research Centre Geesthacht
Institute of Materials Research
Max-Planck-Str. 1, 21502 Geesthacht, Germany

Abstract

The residual strength of a flat panel (thickness 7.6 mm) with five stringers, machined from a monolithic block of Al 2024-T351 material, which contained a crack that divided the central stringer, was to be predicted during a Round Robin organised by ASTM. The initial crack tips were right ahead of the stringers #2 and #4, respectively, so that crack branching along the skin and into the stringers occurred after initiation. The prediction has been achieved using finite element simulations including crack extension, for which a cohesive model was utilised. Conventional material properties, yield and ultimate strength as well as *experimental results from M(T) specimens in terms of force, COD and Δa*, were given. The residual strength prediction was performed in two steps: First the crack extension parameters for the cohesive model, the cohesive strength, T_0, and the cohesive energy, Γ_0, were determined by numerical reproduction of the *results* of the M(T) specimen. With the optimised parameters, the five-stringer panel was modelled. These steps were conducted by two different finite element models: by a shell and a 3D finite element mesh. It turned out that it is possible to analyse the structure with both models. In the 3D case, the residual strength prediction was conservative and the deviation of the predicted from the experimental value was below 9%. The results of the shell simulation were even closer to the experiment (deviation approximately 3%), but the simulation was non-conservative.

Keywords: Residual strength, cohesive model, thin-walled structure, ductile crack extension, aluminium, stiffened panel, experimental validation

Introduction

Methods of conventional fracture mechanics are successfully used for the assessment of engineering structures for a very long time. In many cases the K concept of linear elastic fracture mechanics extended by plastic zone corrections, in the following called the K_{eff}-concept, which goes back to the 60's [1], is still applied to components due to its high level of standardisation and experience. More recently, methods of elastic-plastic fracture mechanics are applied, often in combination with numerical simulations using the finite element method.

Advanced methods for the prediction of residual strength and thus structural fracture assessment use models for crack extension. One model that has gained increasing attraction is the cohesive model, which is based on an idea proposed by Dugdale [2] and Barenblatt [3] also in the early 60's. The first one, who used the cohesive model in combination with the finite element method for the simulation of ductile failure in metals, was Needleman in 1987 [4]. The application to the assessment of metallic structures has been focused in several publications, see e.g. [5], [6].

Naturally, due to computational limitations, the cohesive model has been used for two-dimensional simulations first, but in the late 90's, when computers became more powerful, 3D simulations were performed as well [7], [8], [9], [10], which gave a more realistic

approximation of the processes ahead of the crack tip. For example, the numerical reproduction of crack front tunnelling as shown in [10], is only possible by a 3D analysis.

Thin-walled structures are also a point of interest since a couple of years, and so cohesive elements have been developed for plane stress and shell elements. The problem with these types of structures is that the thickness change cannot directly be accounted for in the cohesive elements, since the interface only consists of a line, which by definition has no thickness. One approach to overcome this problem is to model the row of continuum elements adjacent to the cohesive interface line as plane strain elements. An application of this approach to thin aluminium fracture specimens is presented in [11], [12]. Later on, cohesive elements have been developed that were able to take the actual thickness of the adjacent plane stress or shell elements into account. This has been done by different groups, see e.g. [13], [14], [15], [16].

Even though the cohesive model is in a state, in which it can be applied to complex engineering structures, this application field has gained only very little attention, see e.g. [17]. Therefore, the current investigation is aimed at demonstrating the applicability to components, for which the standard fracture mechanics procedures (see e.g. [18]) cannot be applied with sufficient accuracy.

The structure under investigation is a five-stringer panel, which is part of an ongoing Round Robin organised by ASTM [19]. During the first phase of the Round Robin, three different panels machined from a monolithic Al 2024-T351 block, had to be analysed with respect to fatigue crack growth, but only one of them, shown in Figure 1, was tested for residual strength afterwards. The load was applied to the grip ends shown in the figure under displacement control.

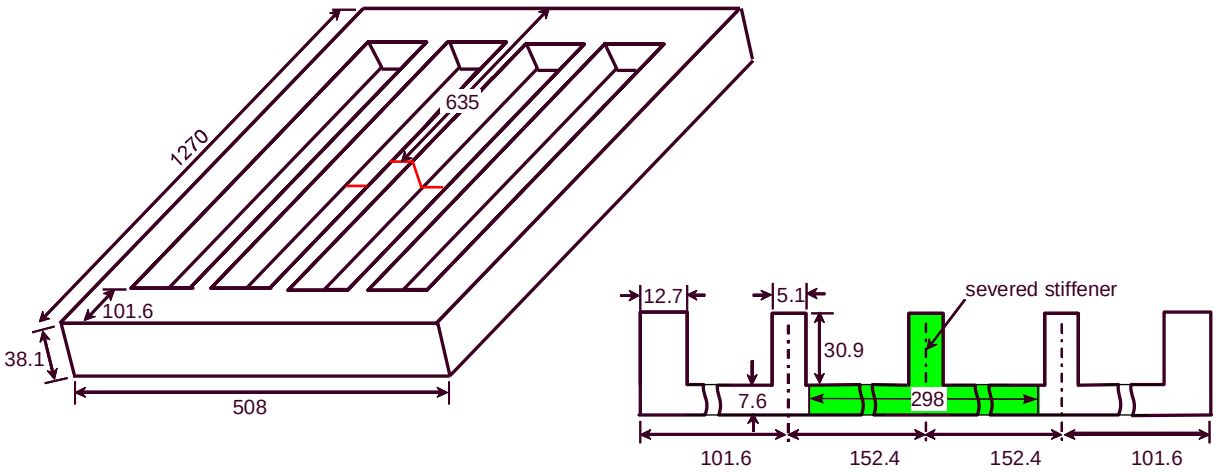

Figure 1: Five-stringer panel containing a crack that divides the central stringer. All dimensions in mm.

The rolling direction is the direction of the stringers, so that the crack configuration can be regarded as L-T orientation.

As displayed in the figure, the thickness of the main panel is almost 8 mm, and therefore the question is raised whether the component is really a thin-walled structure. Since there are several explanations for "thin-walled", it should be defined beforehand. Three different types of definitions exist [20]:

Geometrical definition: A structure is called *thin-walled*, if the thickness is much (e.g. more than ten times) smaller then all other relevant dimensions, which is usually expressed in its slenderness ratio, β.

According to this definition, the panel can be called thin-walled, even though the stringer height is only 6 times larger than its thickness, since the skin length to thickness ratio is more than 10.

Mechanical definition: A structure can be regarded as *thin-walled*, if the stresses in thickness direction are negligible compared to all other stress components (plane-stress assumption).

Especially at the junction between skin and stringer (directly ahead of the crack tip), there might be a local highly constrained area with a complex three-dimensional stress state. This question is very important for the application of shell elements in the numerical analyses.

Structural definition: Design engineers may call a structure thin-walled if it can only carry the applied load by stiffening elements either by use of extra material (reinforcements and ribs) or by design principles (e.g. including optimal curvature or folds) in order to avoid buckling problems.

According to the latter definition, the component is definitely a thin-walled structure.

Numerical Model

As outlined already, the cohesive model is utilised for the numerical crack extension analyses. Arbitrary material decohesion processes are idealised in this model by reducing the fracture process zone to an interface with zero width. Cohesive elements have been implemented as user-defined elements within the finite element code ABAQUS, which obey a so-called traction-separation law (TSL) as a constitutive behaviour that relates the displacement jump vector between the two sides of the element, $\boldsymbol{\delta}$, to the traction vector, $\mathbf{T}(\boldsymbol{\delta})$, acting on the surface. In many cases the one-dimensional representation of the relation is sufficient, namely when only mode I fracture is concerned. The constitutive behaviour can then be written in the form $T_N = f(\delta_N)$, in which the subscript N denotes the normal component of the separation and traction, respectively (and will be omitted further on). Many different laws have been used in the literature, see e.g. the overview given in [22]. The effect of the shape on the crack extension results are discussed e.g. in [23]. In the present investigation the function f is described by the following equation [21]:

$$T = T_0 f(\delta) = T_0 \begin{cases} 2\left(\frac{\delta}{\delta_1}\right) - \left(\frac{\delta}{\delta_1}\right)^2 & \delta < \delta_1 \\ 1 & \delta_1 < \delta < \delta_2 \\ 2\left(\frac{\delta - \delta_2}{\delta_0 - \delta_2}\right)^3 - 3\left(\frac{\delta - \delta_2}{\delta_0 - \delta_2}\right)^2 + 1 & \delta_2 < \delta < \delta_0 \end{cases} \tag{1}$$

The shape of eq. (1) is shown in Figure 2. Alternatively, it can be given in tabular form in order to define an arbitrary shape of the traction-separation law, which will also be used in this study. It is assumed that the traction-separation law has a high stiffness in the beginning, $\delta_1 = 0.01\ \delta_0$, and contains a significant part with a constant stress, $\delta_2 = 0.75\ \delta_0$.

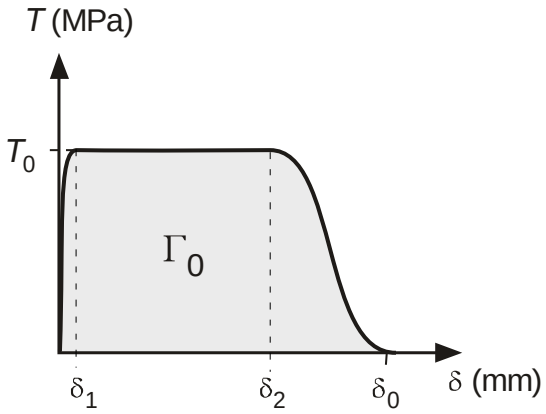

Figure 2: Shape of the traction-separation law as described by eq. (1).

An extension to arbitrary separation processes may be realised by

$$T_I = T_{0,I}\, f(\delta_I)\sqrt{g(\delta_{II})g(\delta_{III})}\ ,\ (I \neq II \neq III) \qquad (2)$$

where indices *I,II,III* stand for different fracture modes (normal, in-plane and out-of-plane shear), and the function *g* describes the interaction between different fracture modes, see also [21]. This multiplicative decomposition of the interaction law is advantageous for an independent choice of the separation behaviour of a single fracture mode and the mode interaction.

The interface elements are available for 2D (plane strain and plane stress), axisymmetric, shell and 3D finite element models. Since the structure under investigation is a complex thin-walled one, the only choice is between shell and 3D modelling. The cohesive elements for shells are of line shape, such that the upper and the lower lines are defined by two nodes each. In the undeformed state these lines are on top of each other, i.e. they do not span a finite area. In order to define the in-plane direction in the three-dimensional space, a fifth node belongs to the cohesive element, see the left sketch in Figure 3. As already pointed out, the cohesive shell interface cannot account for a thickness change if this information is not transferred from the adjacent continuum element. However, the current implementation allows for transferring the out-of-plane deformation to the cohesive element by internal variables via user programming, see [14].

For three-dimensional structures, the interface is defined by 2D elements with 8 nodes, which again do not span a volume in the undeformed state, see the right sketch of Figure 3.

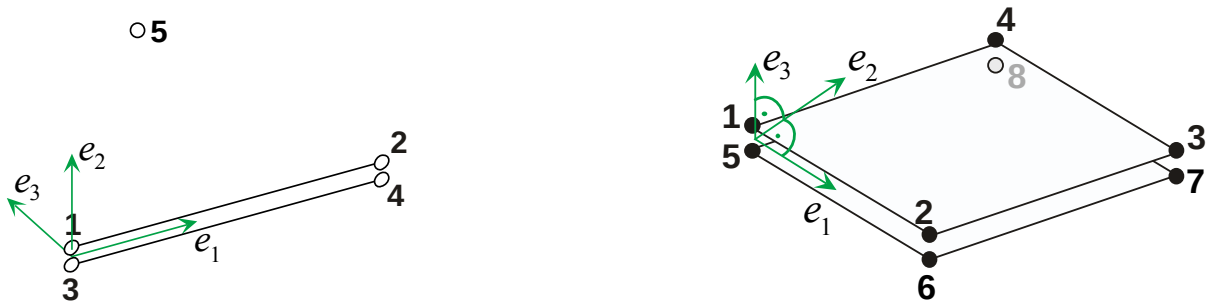

Figure 3: Cohesive elements for shell (left) and three-dimensional models (right).

Experimental Data

In order to determine the residual strength of the stiffened panel shown in Figure 1, it is necessary to identify the properties of the material first. These properties can be divided in two groups: deformation properties, i.e. the stress-strain curve, and fracture parameters.

The elastic-plastic properties have been described by three distinct values, given for two different material directions, see Table 1. The data was given to the participants by the organisers of the Round Robin without any information on how they were determined.

Table 1: Experimental stress-strain data given by ASTM for the Al 2024 material.

	Longitudinal direction (L)	Transverse direction (T)
Yield strength σ_Y [MPa]:	388	342
Ultimate tensile strength R_m [MPa]:	490	485
% Elongation (eng. strain) at R_m:	17.3	18.3

Even though it is known that the cohesive model is very sensitive to changes in elastic-plastic properties and the values given in Table 1 are by far not sufficient for a precise description of the stress state around the crack tip, no alternative was possible from generating a material flow curve from these values.

From the table, one can see that the orientation dependence regarding yield strength and hardening is rather pronounced. However, in ABAQUS, only Hill's anisotropic yield function is available, which does not account for an orientation dependent hardening. Since no appropriate model is available and the aim of the study is to predict the residual strength with the lowest effort possible, isotropic von Mises plasticity is used in all simulations.

Due to the higher hardening in the transverse direction, which leads to higher stresses at the crack tip despite the lower yield strength, it is assumed that using the parameters for this orientation leads to a higher extension rate in the simulation and thus conservative results.

For the generation of a stress-strain curve, the engineering values given in Table 1 first were converted in true-stress – log-strain values, and then a power-law fit was employed to connect the yield and the ultimate tensile point. This constructed curve, which is described by one of the two formulae in eq. (3)

$$\sigma_{true} = \sigma_{Y,0}\left(\frac{\varepsilon}{\varepsilon_Y}\right)^n = \begin{cases} 342\text{MPa}\left(\dfrac{\varepsilon}{0.00503}\right)^{0.14745} & \text{transverse dir.} \\ 388\text{MPa}\left(\dfrac{\varepsilon}{0.005706}\right)^{0.1180} & \text{longitudinal dir.} \end{cases} \tag{3}$$

was then used for all subsequent simulations. Both corresponding curves are shown in Figure 4(a). Of course, this is a very rough approximation of the material's behaviour. Therefore, the results of the simulation will be discussed with respect to the choice of the stress strain curve.

The fracture properties of the material were given data determined by a test on an M(T) panel with a width of $2W = 400$ mm, a thickness $t = 6.44$ mm and an initial crack length of $2a_0 = 103$ mm. From this test three different values are measured: the force, F, the crack mouth opening displacement, COD, and the crack extension, Δa, *averaged over the thickness according to ASTM standard and determined by multi specimen technique*. Based on these

values a F(COD) curve, Figure 4(b), and a fracture resistance curve $K(\Delta a)$, Figure 4(c), were provided. Since the use of K for a thin-walled specimen under large scale yielding conditions is questionable, it is not used for the determination of the cohesive parameters and a COD(Δa) curve is used for numerical identification instead.

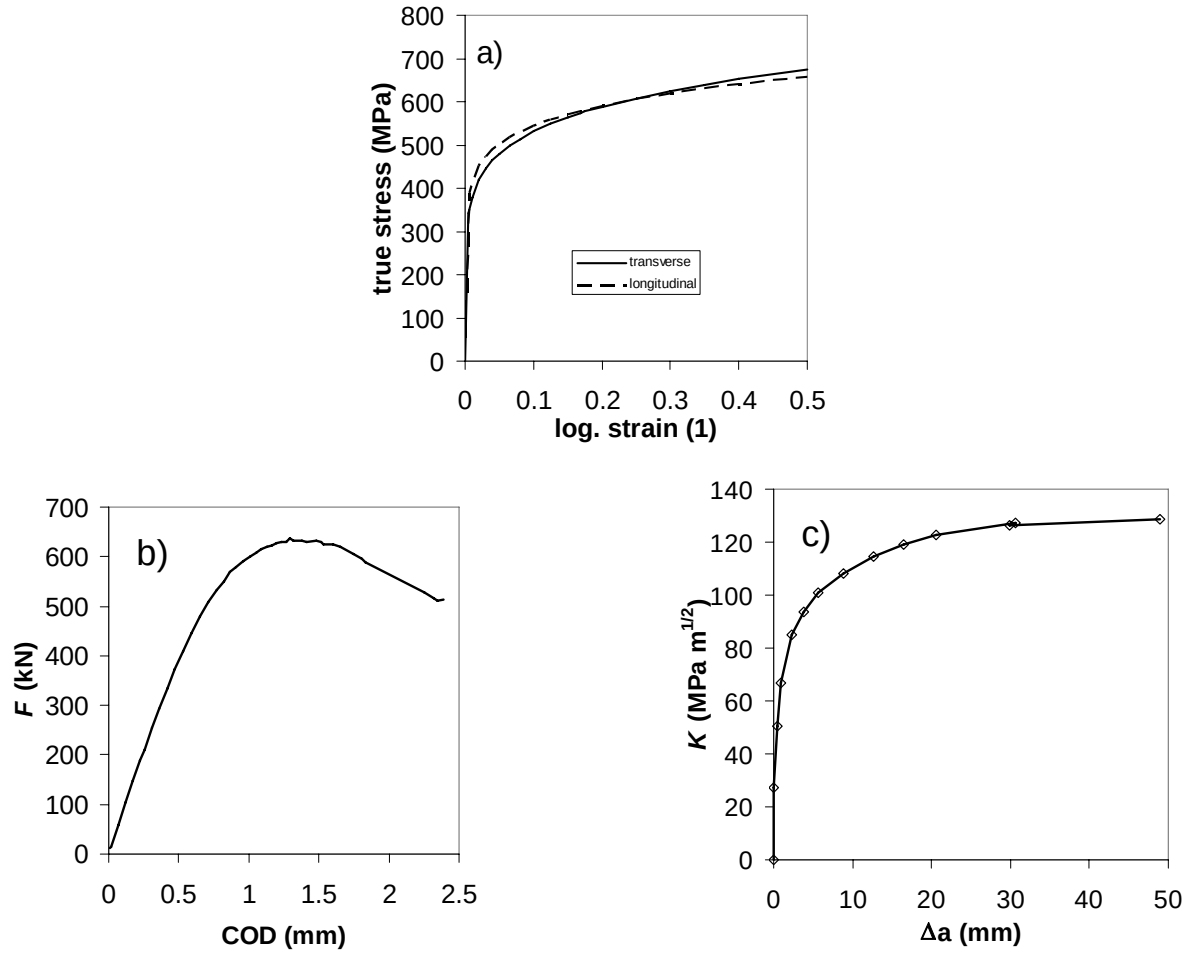

Figure 4: Experimental data given for the characterisation of the deformation and fracture behaviour of the Al 2024 material. (a) True stress-strain curve, generated from the data given in Table 1; (b) F(COD) curve of the M/(T) panel; (c) $K(\Delta a)$ R-curve of the M(T) panel.

Shell finite element modelling

Structures, which might be regarded as thin walled, are commonly modelled by shell elements in industrial applications due to cost and time saving requirements. Therefore the use of shell elements is favoured in the present case.

The task is to predict the mechanical behaviour of the five-stringer panel by numerical simulations. In order to do so, the parameters for the cohesive model have to be identified first, which will be performed by reproducing the experimental F(COD) curve and the COD(Δa) curve of the M(T) specimen. Cohesive parameters are optimised for both stress strain curves given in eq. (3) separately, since cohesive and yield parameters cannot be chosen independently. No optimisation procedure has been employed for their identification, but the adjustment is performed by trial and error instead.

One important point for the transferability of the cohesive parameters is that the fracture mechanisms occurring in the M(T) panel and in the five-stringer panel are identical. It is

assumed that both structures fail by ductile damage and the fracture surface is flat, that is, no slant fracture occurs. It has been assured by the board of the Round Robin that this is the case.

Regarding the numerics, the M(T) panel and the five-stringer panel should be similar in their finite element meshing, namely the same element type (four node shell, ABAQUS designation S4, in the present case) has to be used for both structures and the element size of the cohesive elements should be similar.

Parameter identification

One quarter of the M(T) specimen is to be modelled due to symmetry. The loading is displacement controlled, which is applied at the top nodes of the finite element mesh. A line of cohesive elements is placed along the ligament consisting of 160 cohesive elements with a length of 0.25 mm, thus allowing for 40 mm crack extension. Since the simulation has been stopped after approximately 15 mm crack extension, the number of cohesive elements is sufficient for the development of the cohesive zone.

The mesh shown in Figure 5 consists of 2903 linear shell elements. The total number of degrees of freedom is 18789.

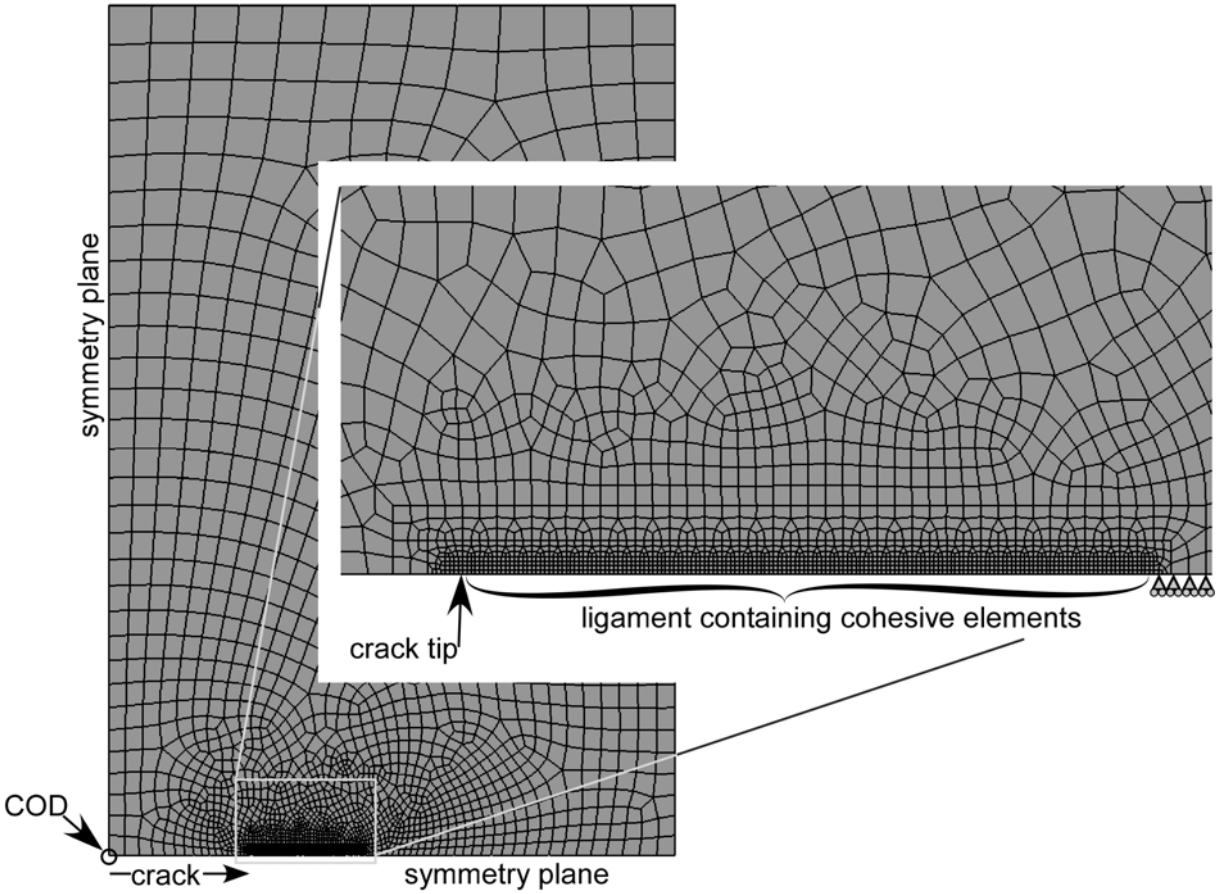

Figure 5: Finite element mesh of the M(T) specimen (one quarter due to symmetry), modelled with shell elements.

Force, COD and crack extension are evaluated and the optimal parameters are identified based on the COD(Δa) curve, leading to $\Gamma_0 = 11$ kJ/m² and $T_0 = 770$ MPa for the stress-strain curve of the transverse direction and $\Gamma_0 = 10.5$ kJ/m² and $T_0 = 795$ MPa for the longitudinal direction. With these values, the critical separation is $\delta_0 = 0.018$ mm and $\delta_0 = 0.017$ mm, respectively. These parameters are reasonable, since tests on similar sheet material (however

with lower yield strength) resulted in slightly lower values of T_0 and Γ_0, see [5]. In addition, Siegmund et al. reported in [11], [13] that a cohesive strength of twice the yield strength is appropriate for sheet material due to the low triaxiality in these structures.

The corresponding curves from the simulation with these parameter sets are shown in Figure 6. From the curves one can see that even though the COD(Da) curves are almost identical, the global force-displacement curve using the stress-strain curve for the transverse direction fits much better to the experiment than that using that for the longitudinal direction. In particular the maximum force, which is the relevant quantity for the prediction of the stiffened panel later on, is overestimated by the latter. Therefore, the former is taken in all future simulations.

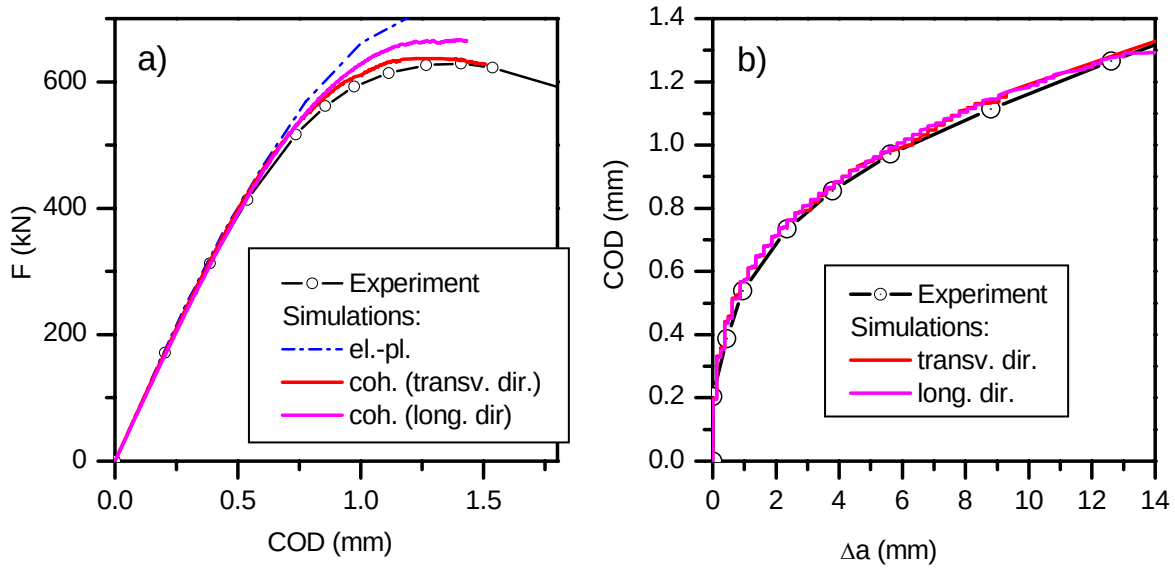

Figure 6: Results for the M(T) specimen, comparison between experiment and simulation. a) F(COD) curve; b) COD(Δa) curve.

Application to the stiffened structure

The parameter identification revealed that both the global F(COD) curve and the COD(Δa) curve can be reproduced and thus the use of shell modelling seems to be possible, and a shell mesh is generated for the five-stringer panel of Figure 1. Due to symmetry only one quarter of the structure is to be modelled. For the sake of simplicity, the shell reference surface is shifted by half the sheet thickness instead of placing it in the centre of the panel in three cases as shown in Figure 7. The clamping region at the top of the structure is assumed to have little effect on the result of the simulation and is therefore not modelled. A vertical displacement is prescribed, instead, where this region begins. The quantities that are evaluated from the simulation are

- force, *F,* and
- crack opening displacement (COD) as shown in Figure 8

The experimental σ_{appl}(COD) curve with $\sigma_{appl} = F/A$ being the applied stress (A = 5110 mm² is the cross section of the uncracked structure), have been provided by ASTM after completion of the round robin for comparison with the numerical results.

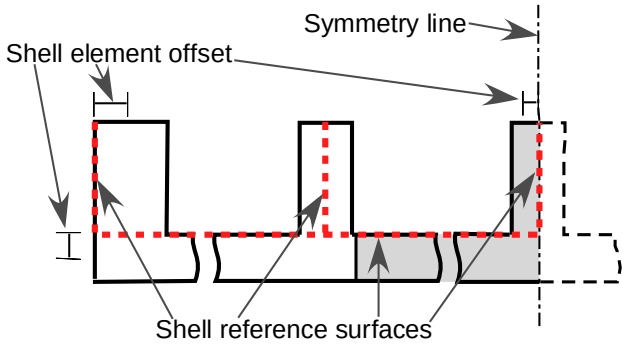

Figure 7: Placement of the shell reference surface (dashed line) with respect to the cross section of the panel.

Shortly after initiation, the crack branches into skin and stringer; therefore cohesive elements must be placed along both lines. Since it is not known how much crack extension can be expected before maximum load, the cohesive elements were placed in the whole stringer and 40 mm along the skin. With a cohesive element length of approx. 0.25 mm this leads to 161 elements along the skin and 102 elements at the stringer. The number of shell elements in the model is 8782, which gives 56070 DOFs in total.

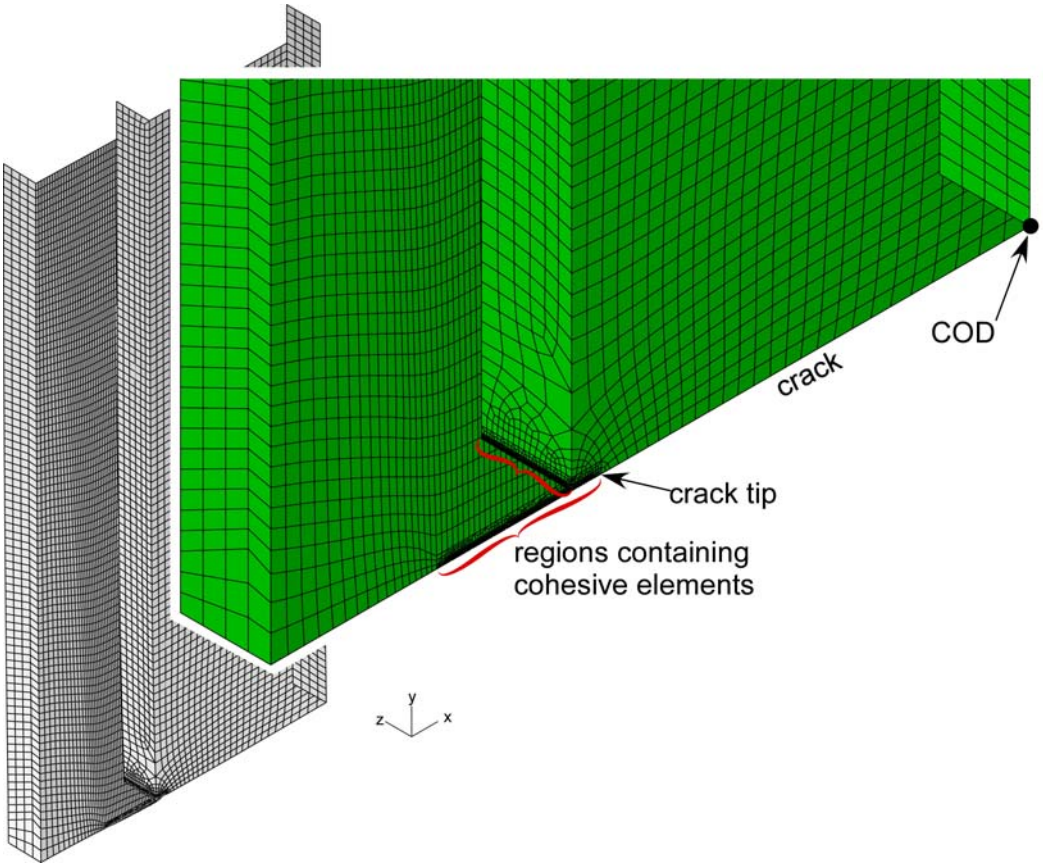

Figure 8: Shell finite element mesh for the five-stringer panel (one quarter of the original structure due to symmetry).

The comparison between experiment and simulation is shown in Figure 9. It turns out that the predicted residual strength is in very good agreement with the experimental value, the difference in maximum applied stress is less than 3% (151 MPa in the simulation instead of 148 MPA in the experiment). It must be mentioned that the numerical prediction is non-

conservative, but it is characteristic for crack extension analyses that no conservatism is ensured.

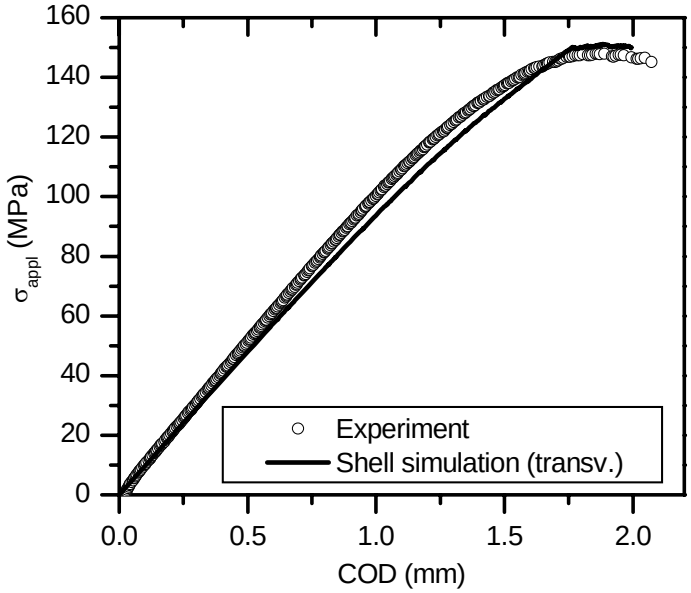

Figure 9: Remote stress versus COD plot of the stiffened panel. Comparison between experiment and shell finite element simulation.

3D finite element modelling

The previous section showed that it is possible to model the five-stringer panel with shell elements. However, in order to discuss the effect of increased triaxiality due to the finite thickness of the structure, it was additionally meshed with 3D continuum elements, even though this means a vast increase in the model size and thus computation time. A small reduction of the problem may be achieved by coupling a 3D mesh for the crack tip region to a shell mesh for the global structure, but since approximately 90% of all elements are placed along the ligament, the savings are not worth the additional meshing effort.

According to the results achieved by Zavattieri [16], which correspond to the authors' experience, the parameters determined by a 3D simulation are different from those determined by a shell simulation. Therefore, if the prediction is performed with a specific element type, the same type has to be used for the parameter identification of the material.

Parameter identification

The 3D FE model of the M(T) specimen represents one eighth of the panel with three symmetry planes and consists of 30408 linear 3D elements (ABAQUS designation C3D8), see Figure 10. 15 layers of solid elements over the half thickness are generated in the ligament, varying between a width of 0.45 mm in the centre and 0.075 mm at the specimen surface, and their length being 0.15 mm in order to keep the aspect ratio of the elements close to 1.0. The cohesive surface consists of 15×200 = 3000 cohesive elements, thus allowing for a maximum crack extension of 30 mm. The whole model has 113472 degrees of freedom.

Again, the stress-strain curve for the transverse direction is used for the deformation behaviour of the structure.

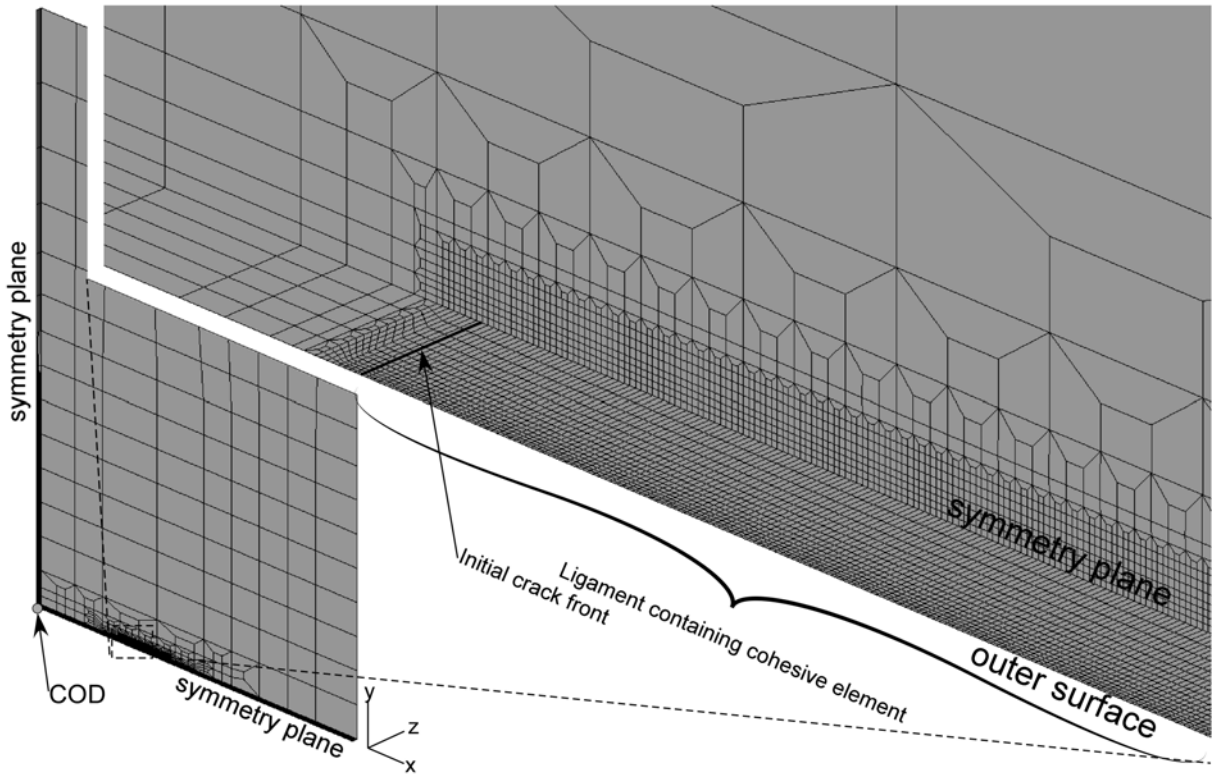

Figure 10: 3D finite element mesh for the M(T) specimen (1/8 of the structure)

The loading is applied by a prescribed displacement at the top of the specimen. As a result, the total force, F, COD and the crack extension, Δa, is determined. The latter is calculated based on the total area of the failed cohesive elements divided by the original thickness. The error due to the deformation of the elements has been assured to be below 5% by calculation on the deformed mesh at a few specific points. The comparisons between simulation and experiment with respect to the F(COD) and COD(Δa) curves are shown in Figure 11. The optimal parameter set for the 3D simulation is $\Gamma_0 = 20$ kJ/m² and $T_0 = 970$ MPa, the critical separation resulting in $\delta_0 = 0.024$ mm. Both the cohesive strength and the cohesive energy are larger than those for the shell simulation. At least for the cohesive strength, this phenomenon has been reported already by Zavattieri [16]. In the respective publication, Zavattieri also showed that this difference in the T_0 value between shell and 3D simulation is dependent on the thickness of the structure, by modelling specimens with sheet thicknesses varying between 1 and 3 mm.

Due to the large computation time, the simulation was stopped after approximately 9 mm of crack extension. At this time, the force was very close to the residual strength of the specimen. Additionally, the results of an elastic-plastic simulation (without crack propagation) are shown in the F(COD) graph. From this curve, the effect of crack propagation becomes evident.

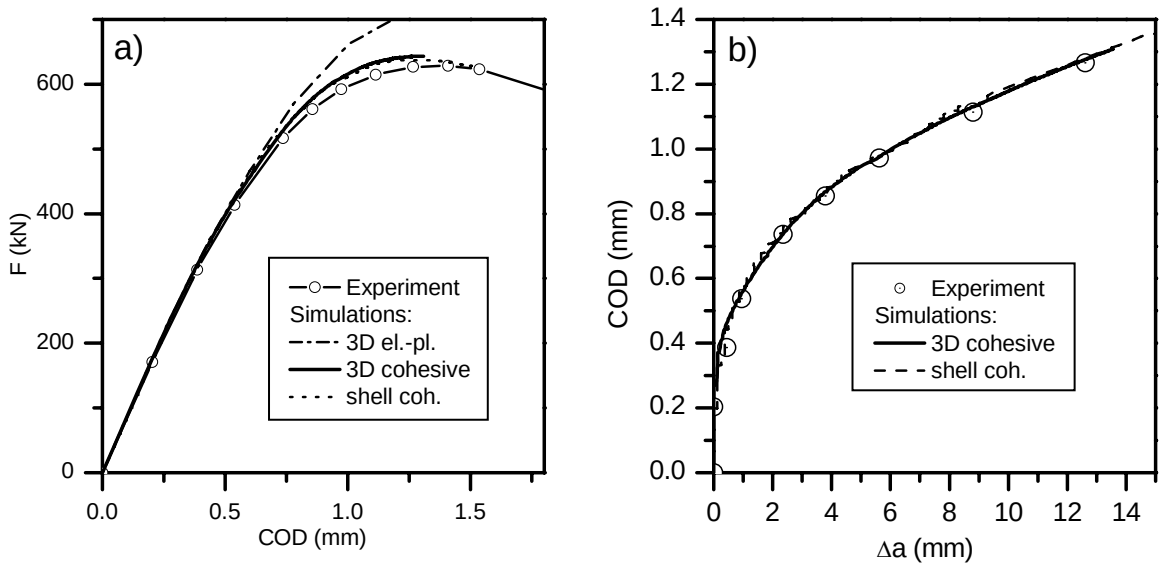

Figure 11: Parameter identification for the 3D FE model of the M(T) specimen. Comparison of simulation and experiment for the respective optimised parameter sets. The shell model simulations are also shown for reference.

The stress state in front of the crack tip is commonly characterised by the triaxiality, defined as

$$h = \frac{\frac{1}{3}\sigma_{kk}}{\sigma_{\mathrm{eq}}} \,, \tag{4}$$

which is shown in Figure 12 at the time of crack initiation (a) and at the end of the simulation (b). One can see that the maximum triaxiality is higher at initiation than at the end of the simulation, but the region of triaxiality $h > 2/3$ (bordered by black lines) increases during crack extension. For a structure under plane stress condition, i.e. the out-of-plane stress component being zero, the triaxiality cannot exceed $h = 2/3$. It is obvious that the actual stress state with a triaxiality up to $h = 1.5$ cannot be characterised locally as plane stress. Even though it was possible to reproduce the results of the M(T) specimen with shell elements (see above), the transferability of the parameters is highly questionable, if the high triaxiality is not taken into account.

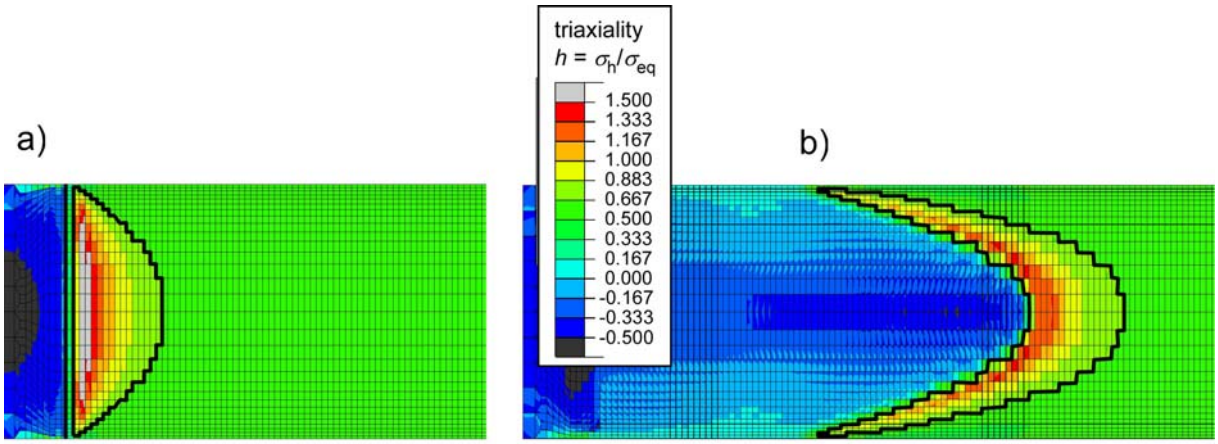

Figure 12: Local triaxiality of the M(T) specimen ahead of the crack tip. a) at crack initiation; b) at end of simulation. The thicker black polygon indicates the region in which the triaxiality is higher than 2/3. (The structure is mirrored by postprocessing)

Application to the stiffened structure

A 3D finite element model containing one quarter of the whole structure, shown in Figure 13, has been generated. The same region as for the shell mesh has been supplied with cohesive elements, but now 15 elements over the stringer thickness and 24 over the skin thickness are introduced, which leads to 4625 cohesive elements in total with a size of approx. 0.3×0.3 mm² each. The part of the ligament mesh allotted for crack extension is displayed in Figure 14. The whole structure contains 41294 3D elements and has 170397 DOFs. The high computation time is not only a consequence of the model size, but also the number of elements, which fail before maximum load. Figure 14 shows the crack extension at the end of the simulation, where approximately 1400 cohesive elements have exceeded the critical separation, δ_0. For this amount of crack growth, more than 6800 increments were needed, for which the simulation took several days on a computer with four AMD Opteron CPUs under Linux.

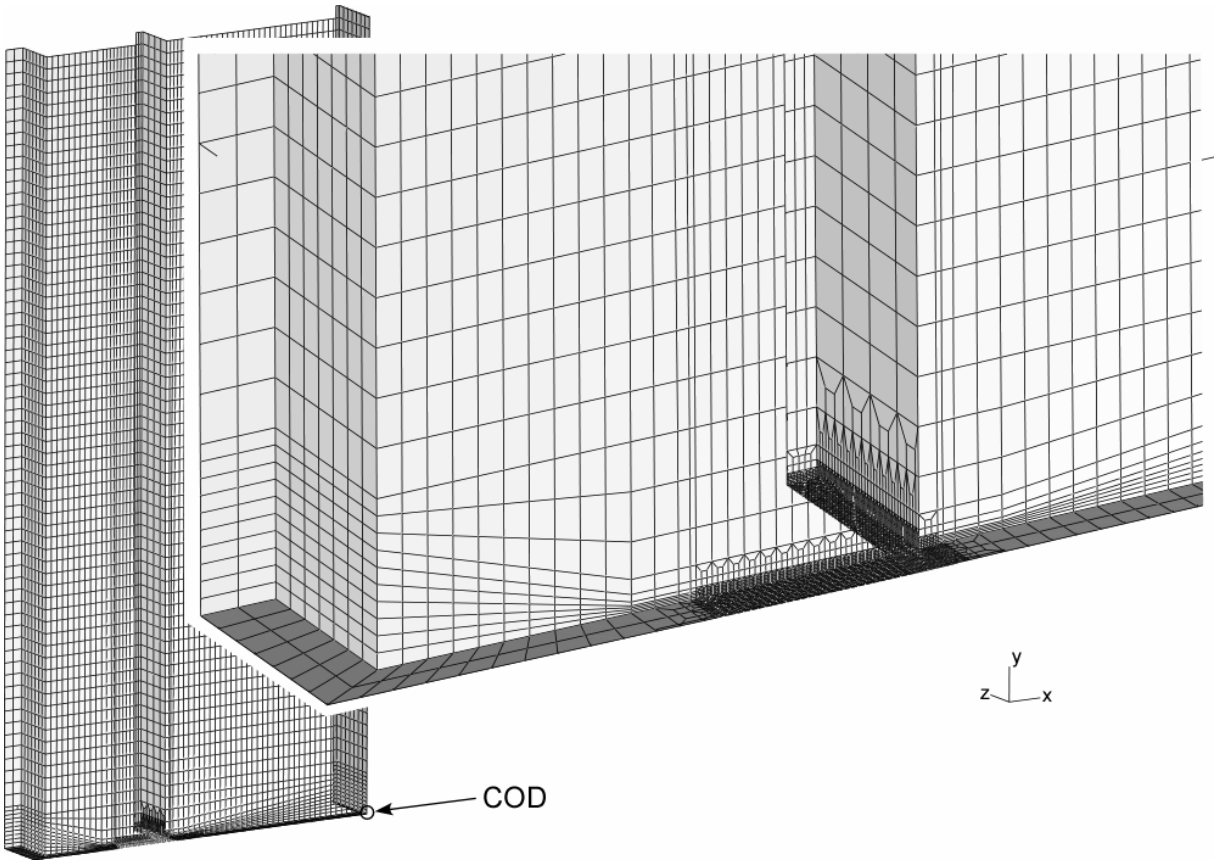

Figure 13: 3D finite element mesh for the five-stringer panel (one quarter due to symmetry).

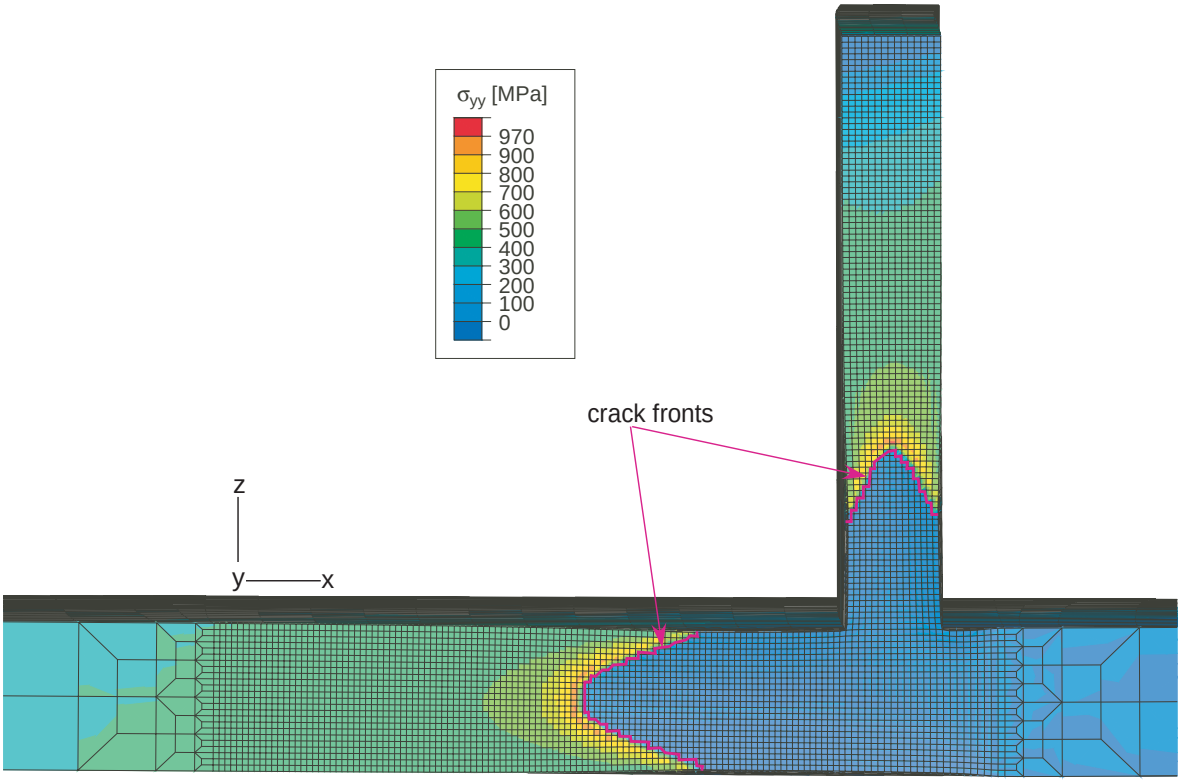

Figure 14: View of the ligament with iso-planes of normal stresses, σ_{yy}, at load maximum also showing the crack extension.

The comparison of the simulation with the experiment is shown in Figure 15. The residual strength in the simulation is 135 MPa compared to 148 MPa in the experiment, which is a deviation of less than 9%. It is worth noting that the prediction is conservative in the present case, which is an important point in structural assessment. However, it is not assured in general that the method will always yield conservative results.

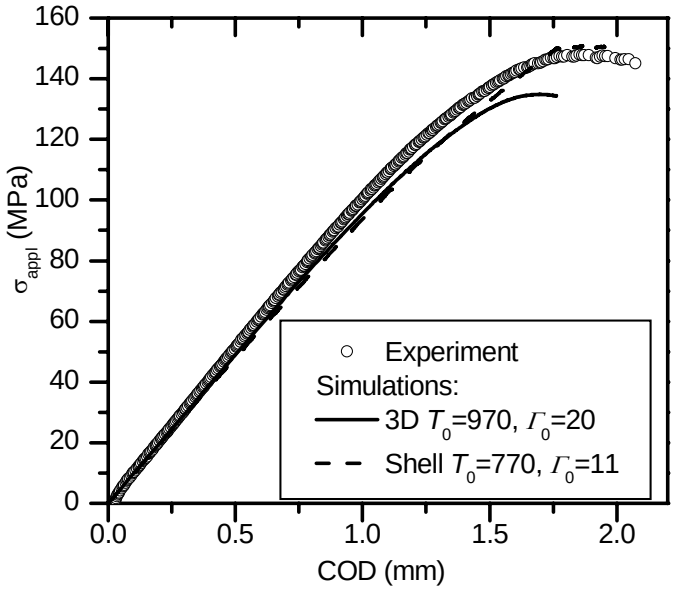

Figure 15: Comparison of the global applied stress vs. COD curves between experiment and 3D simulation (shell simulation shown for comparison).

A comparison between the triaxiality in the M(T) specimen, Figure 12, and the five-stringer-panel, Figure 16, reveals the following: at crack initiation, Figure 16a, the highest triaxiality is very similar to that observed for the M(T) specimen, but the highly constrained region, $h = 2/3$ is more than twice as large as for the M(T) specimen due to the stringer. When the crack reaches the junction, Figure 16b, the region with very high triaxiality, $h > 1.5$, increases significantly (100% compared to Figure 16a) and the size of the region with $h > 2/3$ increases slightly (20%). When the crack front has passed the junction, Figure 16c, the stress triaxiality looks very similar to the one shown in Figure 12b for the M(T) specimen, but the high triaxiality region in the skin is by one third larger than that of Figure 12b.

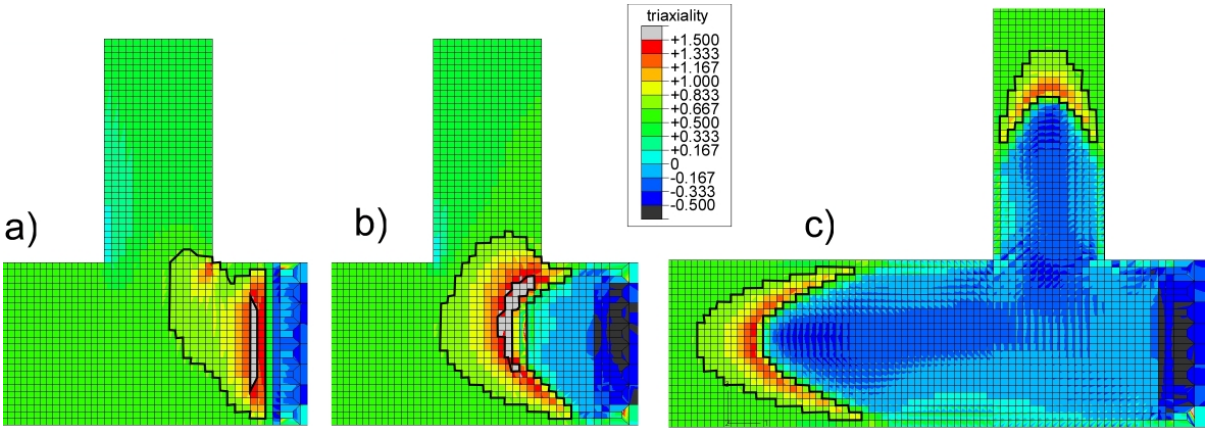

Figure 16: Stress triaxiality at the crack tip for three different deformation levels. a) at crack initiation; b) when the crack reaches the junction; c) at maximum load. The regions with $h > 2/3$ are bordered by black lines, areas with $h > 1.5$ are shown in grey.

Shell modelling using a so-called "effective traction-separation law" approach

It was shown in the previous sections that the shell simulation of fracture specimens and cracked structures is not straightforward due to the constraint ahead of the crack tip. Zavattieri [16], who investigated even thinner specimens (between 1 and 3 mm thickness) by shell model simulations tried to extract the separation properties for the shell model from a 3D analysis. By this approach, only the simulation of the M(T) specimen is to be performed in 3D, and then the corresponding parameters and the shape of the traction-separation law for a shell simulation are calculated based on these simulation results. The method and its application to the present structure are described in the following.

The tunnelling, that is the difference between crack extension in the centre compared to the surface, is around 6 mm at the end of the simulation as shown for example in Figure 12, even though the M(T) specimen is only 6.44 mm thick. In order to generate a traction-separation law for 2D shell models based on 3D simulation results, Zavattieri proposed to average the stress values over the thickness. This is done here along several lines as those drawn into the contour plot of Figure 17, giving $\sigma_{yy,avg}(x,t)$, x being the ligament coordinate (actually the quantities have been evaluated at each row of elements – the lines shown in Figure 17 are only for visualisation purposes). Stress oscillations in the figure come from extrapolation errors of the post processor (steep gradients may lead to large error values).

The same procedure is repeated with the corresponding displacements along these lines, and the average values, $u_{y,avg}(x,t)$ are calculated.

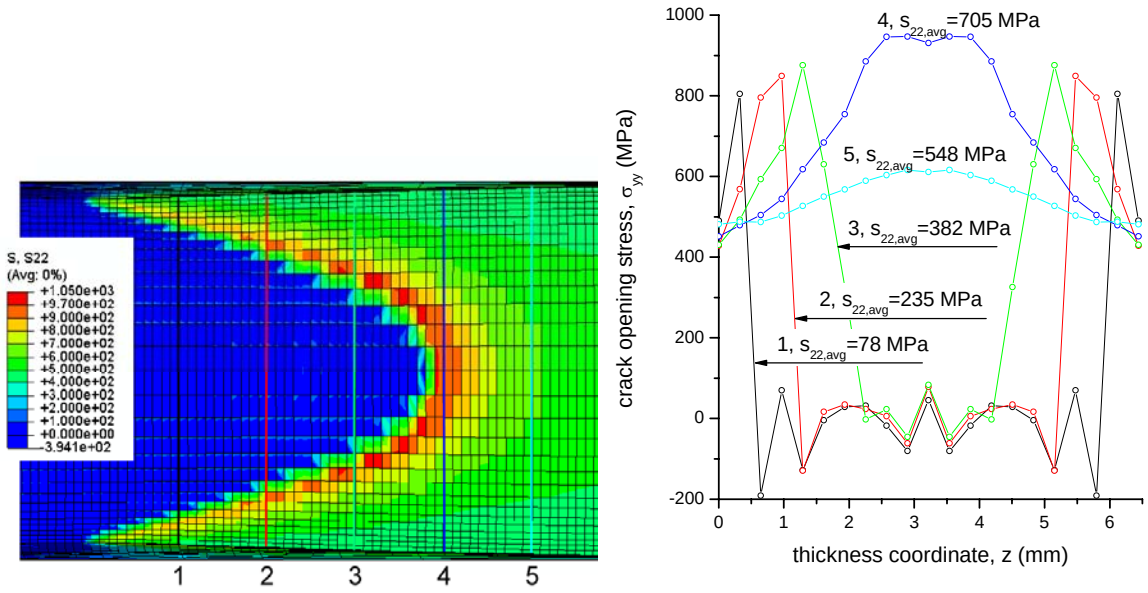

Figure 17: Crack opening stress distribution ahead of the crack tip in the M(T) specimen at maximum load (left, mirrored by postprocessing), and stress distribution along 5 distinct lines with their average values.

The stresses are then plotted versus the displacements, leading to a so-called *effective traction-separation law*, see Figure 18. It turns out that the respective cohesive strength is even smaller than the value that was determined by parameter fitting applying the traction-separation law of eq. (1) for the shell structure, namely $T_0 = 700$ MPa, whereas the separation energy is much larger, $\Gamma_0 = 23$ kJ/m², which gives a very high critical separation of $\delta_0 = 0.113$ mm (more than five times the separation determined by parameter fitting). The traction-separation laws for the 3D and for the shell simulation are drawn in Figure 18 for comparison. The trend is similar to the findings of Zavattieri, which are shown in the upper right corner of Figure 18; in his case the cohesive strength achieved by the effective traction-separation law approach was close to the one that was determined by parameter fitting for the shell model. In addition the critical separation increased significantly (by a factor of approx. two). It should be mentioned that Zavattieri's traction-separation law for the 3D simulation was different from the one used here; the shape was a so-called triangular one, with a steep linear increase and subsequent linear decrease of the traction.

The simulation results based on the generated effective traction-separation law are shown in Figure 19. For the present specimen, the procedure underestimates the residual strength significantly. Zavattieri only stated in [16] that "the crack extension and applied force were not as accurate as the results obtained with the calibrated cohesive parameters" without showing any curve.

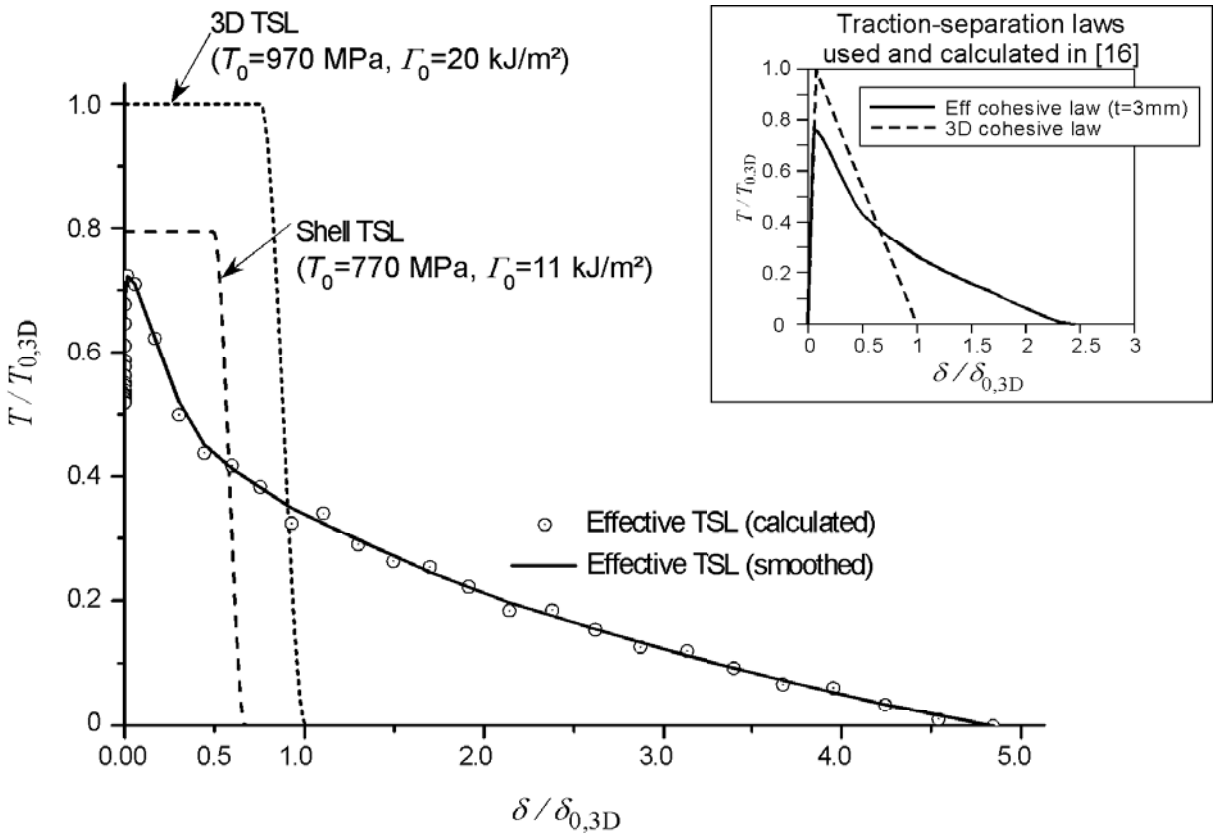

Figure 18: Effective tractions separation law calculated by averaging the stress and displacement of the 3D simulation over the thickness, compared to tractions separation curves for the 3D and the conventional shell simulation. In the upper right corner: Effective and 3D traction separation law used in [16].

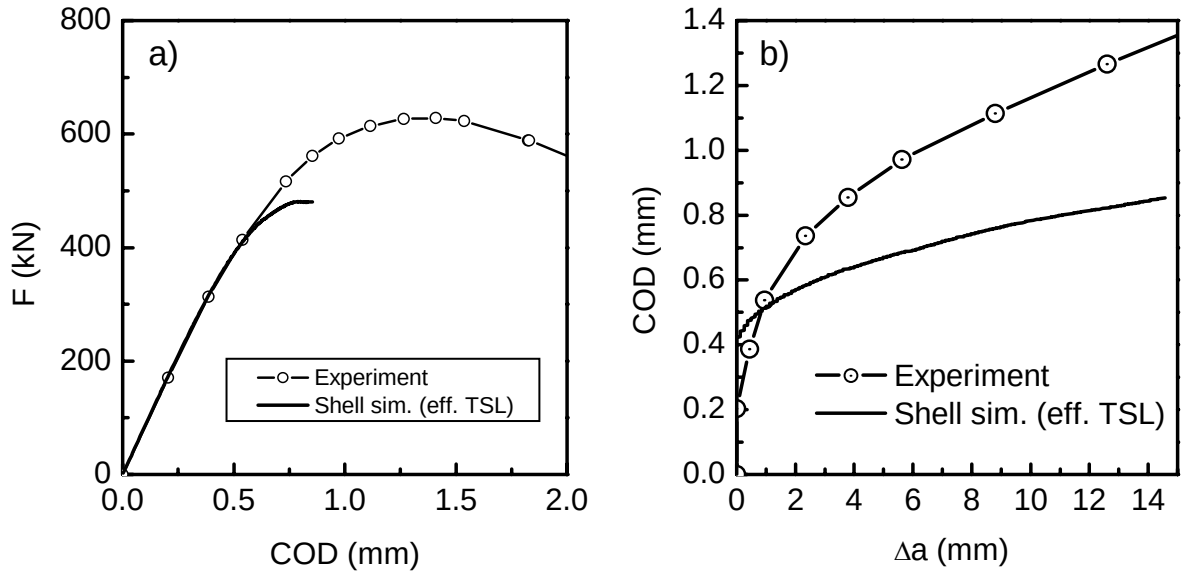

Figure 19: Comparison of experiment and simulation (the latter performed using the effective traction-separation law shown in Figure 18) for the M(T) specimen. a) Force(COD) curve. b) COD(Δa) curve.

The significant differences can be explained by the parameter values and the shape of the traction-separation law: It was shown e.g. in [5], [6], [23] that the crack initiation is governed by the cohesive energy, Γ_0, which is much higher for the effective traction-separation law compared to the respective value obtained from fitting the shell simulation to the experiment, whereas the slope of the crack resistance curve is mainly affected by the cohesive strength, T_0, which is lower here than in the original shell simulation. Furthermore, it has been shown in

[23] that the crack resistance in a simulation may depend on the shape of the separation law: According to the latter investigation, an (almost) rectangular shape yields a higher crack resistance than a triangular or even hyperbolic (concave) shape, if both the cohesive energy and the cohesive strength are kept constant.

The shape and the low T_0 value lead to the relatively flat R-curve behaviour displayed in the left graph of Figure 19, whereas the high cohesive energy, Γ_0, delays the crack initiation. Due to the deviations to the experimental curve, the effective traction-separation law approach cannot be used in the present case. Thus there is still no way of converting the cohesive parameters for different element types.

Conclusions

It has been shown that the cohesive model is able to predict crack extension and residual strength of a complex structure. The approach follows a two-step procedure: First the cohesive parameters have been determined by simulation of an M(T) specimen and fitting of the global force-displacement curve and a COD(Δa) curve to the experiment, and subsequently a five-stringer panel has been simulated with the optimised parameter set. The results show that the parameters can be transferred from fracture mechanics specimens to structures and yield realistic predictions.

The residual strength has been predicted by three participants in a Round Robin organised by ASTM. Two used a *J*-integral approach for the assessment, but the cohesive-model simulation presented here was closest to the experimental result; the maximum stress in the simulation was 135 MPa for the 3D simulation and 151 MPA for the shell simulation (compared to 148 MPa in the experiment), whereas the other two participants predicted 129 MPa and 120 MPa, respectively. However, all simulations but the one with the shell model yielded conservative values of the residual strength.

The predictions based on conventional fracture mechanics parameters as J or K_{eff} face several problems: Firstly, J as a path integral cannot be calculated when structural or material inhomogeneities are present close to the crack tip, which is the case here due to the stringer connection. Likewise the stress intensity factor cannot be calculated since there is no valid K field in the neighbourhood of the stringer connection. In addition, no analytical solutions exist for fracture mechanics parameters in stiffened panels, if the crack approaches the joint. On the other hand, if the crack is located at some distance to the connection, the influence of the stiffener on the crack driving force can be taken into account in analytical methods as well, see e.g. [24]

The cohesive model is able to describe any kind of material separation, even without a pre-existing crack, and therefore no restrictions exist due to non-existing or non-valid fracture parameters. Therefore, the main advantage is not mainly a higher accuracy compared to conventional fracture mechanics analyses, but the ability to predict complex geometries and crack shapes. Another argument in favour of this model is that local variation of the material properties as weldments with different yielding behaviour or residual stresses can be considered in a simple way within the numerical analysis.

It must be noted that the cohesive model is very sensitive with respect to the input data, namely the plastic hardening and the cohesive parameters. In the present case, the small number of data, which was given in the Round Robin (only yield and ultimate strength, and strain at ultimate strength were provided), increases the uncertainty of the results, such that an accurate prediction was not expected at all. However, the demand for accurate input parameters is common to any kind of residual strength prediction. The different accuracy levels in analytical procedures, see e.g. [24], are distinguished mainly by an increasing

number of required input parameters. In order to achieve conservative results, the stress strain curve leading to the lowest residual strength has been taken for all simulations. This is probably one reason for the deviation between 3D simulation and experiment For better results it is recommended to use an appropriate plasticity model as proposed for example by Bron and Besson [26], which is able to reproduce the deformation behaviour accurately. In the case of Aluminium as used in the present study, the anisotropy cannot be captured by the most simple Hill model, and no other model is implemented in the finite element software ABAQUS so far. Most industrial companies are not able to implement high sophisticated material models into finite element codes and therefore the use of von Mises plasticity is justified from the engineer's point of view.

One important point is the applicability of shell meshes to thin walled structures containing cracks. Even though the global behaviour of the present structure is mainly plane stress and the panel might be regarded as thin-walled based on its slenderness ratio, it has been shown that the stress state in front of the crack tip contains a region with a triaxiality higher than $h = 1.5$. Such high triaxialities cannot be accounted for by a shell theory, and therefore the results for the shell simulation differ by more than 10% from those of the 3D simulation. However, the results are still in very good agreement with the experiment.

Recently, transferability has been shown from C(T) specimens to M(T) and cruciform specimens for 3 mm thick aluminium material, see [15]. Further validation seems appropriate on this issue to define a criterion for the applicability of shell meshes to slender structures.

The 3D simulation was rather costly in terms of meshing and simulation time, indeed, but the good agreement between experiment and simulation justifies the effort. The amount of crack extension before maximum load may be very large especially in thin walled structures, such that many (in the present case more than 4500) cohesive elements had to be inserted into the model, but computer power is steadily increasing and therefore this issue will diminish in the future. In [25] it is shown that crack extension of 50 mm and even more is already possible in a large fuselage panel today.

Beside the principal applicability of the cohesive model to crack extension predictions in arbitrary structures, another advantage of the numerical investigation is that not only the residual strength is calculated, but simultaneously a stress analysis of the structure is delivered, which was used in the present case to determine the stress triaxiality in the crack tip region, for example.

Unfortunately the promising method for the determination of an effective traction-separation law for shell models based on an average of the stress state in the 3D crack extension simulation presented by Zavattieri [16] was not successful in the present case. The parameters and the shape of the traction-separation law generated by that procedure are such that crack initiation is delayed, but the crack extension rate (in terms of $\partial a/\partial COD$) is too high.

The reason might be that the cohesive strength is reduced by averaging the stresses over the thickness, since regions of high and low stresses are mixed due to the tunnelling of the crack, whereas the peak stress must be overcome at any material point in a 3D simulation.

References

[1] G. Irwin, Structural aspects of brittle fracture, *Appl. Mat. Res.* **3**, 1964, 65-81

[2] D. S. Dugdale, Yielding of steel sheets containing slits, J. mech. Phys. Solids **8**, 1960, 100-108.

[3] G. I. Barenblatt, The mathematical theory of equilibrium of cracks in brittle fracture, *Adv. Appl. Mech.* **7**, 1962, 55-129.

[4] A. Needleman, A continuum model for void nucleation by inclusion debonding. *J. Appl. Mech.* **54**, 1987, 525-531.

[5] A. Cornec, I. Scheider, K.-H. Schwalbe, On the practical application of the cohesive model, *Eng. Fract. Mech.* **70**, 1963-1987, 2003.

[6] H. Yuan, G. Lin and A. Cornec, Verification of a cohesive zone model for ductile fracture. *J Engng Mater Technol.* **118**, 1996, 192–200.

[7] G. Lin, A. Cornec and K.-H. Schwalbe, Three-dimensional finite element simulation of crack extension in aluminium alloy 2024-FC. *Fatigue Fract. Engng. Mat. Struct.* **21**, 1998, 1159-1173.

[8] G. Ruiz, A. Pandolfi and M. Ortiz. Three-dimensional cohesive modelling of dynamic mixed-mode fracture. *Int J Numer. Meth. Engng*. **52**, 2001, 97–120.

[9] Y. A. Roy and R. H. Dodds, Simulation of ductile crack growth in thin aluminium panels using 3-D surface cohesive elements. *Int. J. Fracture* **111**, 2001, 21-45.

[10] C. R. Chen, O. Kolednik, I. Scheider, T. Siegmund, A. Tatschl and F. D. Fischer, On the determination of the cohesive zone parameters for the modeling of micro-ductile crack growth in thick specimens. *Int. J. Fracture* **120**, 2003, 517-536.

[11] T. Siegmund, W. Brocks, J. Heerens, G. Tempus and W. Zink, Modeling of crack growth in thin sheet aluminium. In "*ASME Int. Mechanical Engineering Congress and Exposition: Recent Advances in Solids and Structures*" Nashville, 1999, 15-22.

[12] O. Chabanet, D. Steglich, J. Besson, V. Heitmann, D. Hellmann and W. Brocks, Predicting crack growth resistance of aluminium sheets. *Comp. Mater. Sci.* **26**, 2003, 1-12.

[13] W. Li, and T. Siegmund, An analysis of crack growth in thin-sheet metal via a cohesive zone model, *Eng. Fract. Mech.* **69**, 2002, 2073-2093.

[14] I. Scheider and W. Brocks, Cohesive model for thin-walled structures, *Comp. Mater. Sci.* **37**, 2006, 101-109.

[15] I. Scheider, M. Schödel, W. Brocks and W. Schönfeld, Crack propagation analyses with CTOA and cohesive model: Comparison and experimental validation, *Eng. Fract. Mech.* **73**, 2006, 252-263.

[16] P. Zavattieri, Modeling of crack propagation in thin-walled structures, *Trans. ASME, J. Appl. Mech.* **73**, 2006, 948-958.

[17] I. Scheider and S. Heartness, Restfestigkeitsanalyse einer Flugzeugrumpfschale mit Hilfe von benutzerdefinierten Kohäsivelementen, Proc. of the 19. German ABAQUS Users' Conference, Erfurt, Germany, 2006.

[18] M. Schödel and U. Zerbst, Application of the European flaw assessment procedure SINTAP to thin wall structures Analytical assessment levels, *Eng. Fract. Mech.* **71**, 2004, 1035-1058.

[19] M. Heinimann and M. James, Analytical Round Robin on Integral Structures, presented at the ASTM E08 Meeting, Dallas, TX, Nov. 2005.

[20] M. Bischoff, W. A. Wall, K.-U. Bletzinger and E. Ramm, Models and Finite Elements for Thin-walled Structures. In: Erwin Stein, René de Borst, Thomas J. R. Hughes (eds.): Encyclopedia of Computational Mechanics, Part 2: Solids and Structures, 2004.

[21] I. Scheider and W. Brocks, Simulation of cup-cone fracture using the cohesive model. *Eng. Fract. Mech.* **70**, 2003, 1943-1961.

[22] W. Brocks, A. Cornec and I. Scheider, Computational aspects of nonlinear fracture mechanics. In: I. Milne, R.O. Ritchie, B. Karihaloo (eds): Comprehensive Structural Integrity, Vol. 3, 2003, 127-209.

[23] I. Scheider, and W. Brocks, The effect of the traction separation law on the results of cohesive zone crack propagation analyses. *Key Engng. Mater.* **251-252**, 2003, 313-318.

[24] U. Zerbst, M. Heinimann, C. Dalle Donne and D. Steglich, Fracture and damage mechanics modelling of thin-walled structures – an overview. *Eng. Fract. Mech.*, this issue, 2007.

[25] A. Cornec, IMA fuselage section modelling. *Eng. Fract. Mech.*, this issue, 2007.

[26] F. Bron and J. Besson, A yield function for anisotropic materials: Application to Aluminum alloys, *Int. J. Plast.* **20**, 2004, 937-963.